"METALLIC" BORON NITRIDE

C SREENIVASULU, C VINOD, K CHENNA REDDY
ASSISTANT PROFESSOR [1,2,3]
chitrasreenu44@gmail.com, vinodatp78@gmail.com, chenna_atp@gmail.com
Depart of chemistry,
Sri Venkateswara Institute of Technology,
N.H 44, Hampapuram, Rapthadu, Anantapuramu, Andhra Pradesh 515722

Presented at 3rd International Conference "Nanotechnologies", October 20 – 24, 2014, Tbilisi, Georgia (Nano – 2014)

Abstract: The synthesis of boron nitride shell structures with a chemical composition of BNx, where x is less than or equal to 1, and carbon is present, involves melting a boron-rich material in a crucible made of boron nitride. The nitrogen source is high-purity pressed boron nitride rods, which supported the crucible. Even though all boron nitrides with a stoichiometric chemical composition of BN are insulators, the produced substance is discovered to be conductive. The structural alterations of semiconducting boron and boron carbide, extensively doped with nitrogen, are combined to form the model of "metallic" boron nitride. According to first principle calculations carried out in the quasi-classical approximation, nitrogen impurities, which are found in all-boron and boron-rich crystalline lattices, cause the local "metallization" of chemical bonds in these structures that were initially covalently bonded by creating donor electron-states inside the conduction band.

Nevertheless, 3D BN might become an innovative material with electrical application possibilities if a method (such as doping) could induce metallicity in these structures. extended beyond the realm of traditional pottery.

The potential for BN's inherent metallicity was a small number of articles.

Keywords: boron nitride, non-stoichiometric chemical composition, metallization by doping.

Introduction

Diatomic molecules, nanotubes, fullerenes, rhombohedral, cubic, and wurtzite-like crystals are all possible structures for boron nitrides, which have the chemical formula BN with a stoichiometric ratio of B:N = 1: 1. Experiment and theory agree that they all have large HOMO-LUMO gaps, or broad bands. Numerous studies have examined their electrical and chemical-bonding characteristics. Using a quasi-classical-type calculation approach, we have specifically examined the electronic structure of the BN diatomic molecule, BN infinite hexagonal sheet, h-BN, c-BN, and w-BN crystals.

Boron nitride, with the molecular formula BN, is a carbon-like compound. In terms of structure, they are quite comparable and share a wide range of dimensionalities: layered crystals and hexagonal sheets, nanotubes and fullerenes, zinc blende and crystals that resemble wutzite. But BN is always an insulator, regardless of structure or dimensions, unlike carbon, which may be metallic. One property that restricts the electrical applications of 3D boron nitrides is their status as broad band gap insulators. metallic structure that resembles white tin was computed for the first mentioning the density-functional-theory (DFT) study7, which indicated that c-BN (111) nanofilms are metallic and transform into semiconductors once their thickness is too little, as regarding the latest calculations, it is worth noting that the reference time is 6. The remarkable metallic behaviour seen in polar nanofilms is not inherent but rather the result of a synergistic impact of thickness-dependent intrinsic electric polarisation and labile near-gap states. A metallic, dynamically stable tetragonal phase of BN has been postulated based on theoretical calculations.8 By examining its band structure, density of states, and electron localization function, the metallic behaviour is proven to originate from the delocalized B 2p electrons.

The density-functional theory (DFT) also revealed a set of 1D nearly-free-electron (NFE) bands of BN nanotubes distributed along the axis of the BN. These nanotubular states are derived from the screening process that determines the image potential of the parent 2D BN sheets. Electrons in nanotubes converge to image potential states when their radius surpasses the radial extent of non-Fermionic states. All of the BN single-walled zigzag nanotubes were found to be semiconducting in nature, according to a comparative DFT analysis in generalized-gradient-approximation (GGA) conducted on their electronic properties. In contrast, the nanotubes of BP and BAs are metallic up to a certain diameter, according to the same analysis. In an expanded attractive Hubbard model, a superconducting state was predicted11 using Green's function method in a zigzag BN nanotube. Nevertheless, point, dot-like, or linear structural flaws are usually associated with the metallicity of boron nitrides with stoichiometric ratios of B:N = 1: 1.

The band gap may be drastically reduced, turning insulator BN nanoribbons into semiconducting ones, by increasing the B-content relative to the N-content, as shown by the DFT using the local-spin-density-approximation (LSDA)12. Specifically, it was anticipated that armchair ribbons with an excess of B-atoms would exhibit a more stable triplet structure while having a greater density-of-states (DOS) around the Fermi level, in the upper valence band. Investigating the impact of vacancies and substitutional defects on the electronic characteristics of h-BN in a two-dimensional molecule model, researchers used density-functional theory (DFT) at the local density-approximation (LDA) level. Their findings revealed that these specific defects narrow the energy gap between the HOMO and LUMO states. DFT simulations using the LSDA14 have shown that N-terminated nanodots and antidots exhibit half-metallicity in triangle-shaped structures such as nanoholes, nanodots, and lattice antidots in h-BN monolayer sheets. The stability and improved half-metallicity of antidot superlattices were expected, even though there was a considerable lattice contraction caused by the presence of numerous holes.

A description was given of the production of BN nanospheres with a rough surface composed of open nanocones and corrugated ribbons. These nanospheres showed remarkably stable field emission capabilities even at low turn-on voltages. As shown by first-principles calculations, these electron emission features are due to the existence of finite BN ribbons with zigzag edges that act like metals. They found that compared to BN-bulk material, the work function of zigzag BN ribbons is lower. The authors said that their paper was the first time the prospect of discovering a metallic form of BN had been discussed. Theoretical evidence derived from total-energy first-principles calculations of the existence of states and extended along the edges of bare zigzag BN-nanoribbons has also been presented.16 Specifically, it was demonstrated that an external electric field could be used to control a wide range of electronic behaviours, leading to metallic semiconducting half-metallic transitions. The ground states of the N-edged ribbons are half-metallic, according to the electronic structure estimates for the zigzag-edged BN nanoribbons performed using density-functional theory (17). Depending on the kind of edge and line defect, the BN nanoribbons with topological line defects display varied electronic characteristics, including half-metallicity and half-semimetallicity, according to first-principles spin-polarized calculations

18. It is also possible to adjust the half-semimetal gap by applying tensile strain. Although line defects divide the BN sheet (or nanotube) into domains, they can lead to edges that significantly reduce the band gap, according to a comprehensive study19 that examines the effects of line defects on electronic properties of monolayer BN sheets, nanoribbons, and single-walled nanotubes using first-principles calculations and Born-Oppenheimer quantum molecular dynamic (MD) simulation. Specifically, it is anticipated that the ground state of the zigzag BN nanoribbons with line defects and all N-terminated edges would be metallic. Using first-principles calculations, the BN stereo-nanoribbons made of three BN ribbon wings joined at the junctions were studied.20 It was discovered that the tri-wing BN nanoribbons may have metals for the zigzag edges or

semiconductors with a small band gap that exhibit metallic behaviours when sp3-bonded junctions are present, depending on the bonding properties. The spontaneous formation of covalent interlayer bonds at the edges of an h-BN bilayer was shown to occur through a combination of TEM data and density-functional theory (DFT) calculations. This led to subångström distortions of the edge's atomic structure, which could be reconstructed to restore the material's bulk-like insulating behaviour and contradict the predicted metallic nature of open edges. The presence of impurities may also affect the metallicity of boron nitrides with a stoichiometric ratio of B:N = 1: 1.

According to the results of the first-principles study22 on the electrical characteristics of BN nanoribbons with H-atom passivated edges, the band gap for these nanoribbons with armchair-shaped edges oscillates with increasing width. While the band gap steadily shrank and converged to 0.70 eV for nanoribbons with zigzag edges, it converges to a constant value of 0.02 eV for broader ribbons. These two numbers, because of the edge-states, are much less than the bulk gap. Using density-functional theory (DFT), researchers were able to determine that the ground states of H-terminated zigzag B-edged BN nanoribbons are half-metallic. Irrespective of ribbon width, completely hydrogenated zigzag BN nanoribbons were determined to be metallic, according to first-principles calculations that examined the fascinating electrical characteristics of fully and partly hydrogenated BN nanoribbons. When the hydrogenated component is prominent, the zigzag BN nanoribbons that are partly hydrogenated show a transition from semiconductor to half-metal to metal. The zigzag-edged BN nanoribbon, which has been experimentally extensively used, exhibits half-metallicity with full hydrogenation and can be tuned by applying a transverse electric bias, according to the DFT-studied electronic characteristics of fully hydrogenated BN layers and zigzag-edged BN nanoribbons. Similarly, few-layer rippled h-BN membranes undergo noticeable changes in their electronic properties after being treated with atomic H-plasma, including a reduced band gap, a sign of transitioning from the insulating to the semiconducting regime.
The band gap was found to be smaller in armchair BN nanoribbons that were edge-terminated with hydroxyl OH-groups or O-atoms according to the DFT-based quantum mechanical description of their electronic properties. However, conventional spin-polarized DFT calculations27,28 revealed that, in contrast to the semiconducting zigzag BN nanoribbons that were H-terminated, the O-terminated ones had two energetically degenerate ground states on the B-edge, both of which were metallic, and all the S-terminated ones were metallic as well. An oxidised hexagonal monolayer of BN supported by a Cu substrate has metallic characteristics when an O adatom forms a vertical link with the B atom, according to first-principles calculations 29. The p-orbital of the BN layer and the O adatom hybridising at the Fermi level is primarily responsible for this. The development of the vertical O-B bond is stabilised by charge transfer from the Cu substrate to the O atom. By injecting negative charges, the oxidised nanosheet may undergo a metallic transition when the O adatom migrates from the B-N bond to the B atom for the supported monolayer.
In order to investigate the electrical characteristics of BN sheets while considering the existence of flaws, DFT was employed30. The building under consideration was a hexagon with three pentagons and three heptagons around it in alternate patterns. The effects of doping were investigated by substituting C atoms for B and N atoms. A semimetal was formed when a C atom was substituted for a B atom. Another way to get a semimetal was to swap out two B atoms for two C atoms. Substituting three carbon atoms for three nitrogen atoms in the centre hexagon transformed the structure into a conductor while keeping its semiconductor properties.
According to research31 that looked at how C-impurity doping affected the h-BN sheet's DOS using both the random tight-binding model and Green's function technique, adding C-atoms lowers the band gap of the BN system and, at high concentrations, makes the DOS of the BN plane look like graphene, leading to semimetallic behaviour. By combining density-functional theory (DFT) with Green's function quasi-particle method, the electronic structure of carbon-doped h-BN sheets was investigated, and a qualitatively accurate description of the impurity states in the gap was provided.
Using Green's function and density-functional theory (DFT), the electronic structures and transport characteristics of fluorinated zigzag-edged BN nanoribbons were studied. The results demonstrated that changing the fluorination level or selecting different fluorination sites can achieve the half-metal to semiconductor transition. Using density-functional theory calculations, a thorough investigation34 was carried out on the semi-fluorinated BN bilayers. Ferromagnetic coupling, which must display half-metallic behaviour for BN bilayers, is favoured by the combined impact of inherent intralayer strain and interlayer charge transfer. A typical semiconductor property was shown by the h-BN nanosheets that were doped with F-atoms35 using a straightforward chemical solution technique with fluoboric acid.
Using density-functional theory (DFT) computations, an investigation36 into the electronic structure of BN nanotubes doped with alkali revealed that the NFE state links with the states of the alkali atoms, producing metallic states close to the Fermi level. The hybridization involves both the s- and d-orbital states to a large extent, and the resultant metallic states maintain an energy dispersion similar to that of free electrons. The main characteristic of alkali-doped BN nanotubes is the nodeless wave function at the Fermi level, which is combined with the decreased work function. The electrical and structural characteristics of BN nanotubes and iron oxide (FeO) monolayers were studied37 using a GGA version of density-functional theory. Their chemical composition changes from a semiconductor to a half-metal or a semimetal to a half-metal when exposed to an electric charge, depending on the tube's diameter.
Lastly, the presence of carbon phase-inclusions may explain why boron nitrides with a stoichiometric ratio of B:N = 1:1 remain metallic.

For hexagonally bonded honeycomb ribbons of B, N, and C atoms, there exist metallic BNC ribbons with various zigzag edges, C and BN or NB, as determined by the first-principles total-energy electronic-structure calculations carried out inside the LSDA38. Additionally, the first-principles study39 indicated that, within a certain width range for the graphene and BN sections, hybrid C/BN nanoribbons with dihydrogenated edges may exhibit half-metallicity.
As the width of the graphene and BN nanoribbons grows, the hybrid C/BN nanoribbons may undergo the semiconductor-to-half-metal-to-metal transitions. The transitions from semiconductors to half-metals to metals may be triggered by the interaction of localised edge states near the Fermi level, which can be induced by dihydrogenation of the B-edge. Using the first-principles nonequilibrium Green's function method, the electrical transport was discovered to be significantly enhanced with a transmission conductance around the Fermi level in hybrid nanoribbons made by partially substituting zigzag BN (or graphene) nanoribbons with zigzag graphene (or BN) nanoribbons. Coupling between B (or N) and C atoms at interfaces, which creates two bonding and antibonding bands around the Fermi level, was thought to be responsible for the improvement in these hybrid systems. The size restriction of half-metallic characteristics in hybrid zigzag BCN nanoribbons was also reported41, based on first-principles calculations. In hybrid systems, the C-segments, not the BN-segments, are the primary determinants of electronic characteristics. As the width of the carbon segment grows, transitions between semiconductor, half-metal, and metal may be realised. A distinct kind of disordered two-dimensional electrical system is formed by atomic layers that comprise hybridised graphene and h-BN domains, also known as h-BNC. Low-temperature magneto-electric transport experiments in vapor-phase synthesised h-BNC layers revealed an unusual and noticeable change from an insulating to a metallic behaviour as the layers cooled down. Electron and hole doping, as well as an external magnetic field, may affect this transition. Based on these findings, which are corroborated by first principles calculations, this transition in h-BNC is presumably caused by the simultaneous presence of percolation via metallic graphene networks and hopping conduction between edge states on insulating h-BN domains that are scattered randomly. The study in ref.43 also looked at the unique electrical characteristics of graphene nanoflakes of different sizes embedded in a BN layer. More specifically, it found that the size of the h-BN triangular clusters within the graphene supercells and the distance between them determine the ability to induce spin polarisation through charge-doping. Certain charged states, which are typically metallic, exhibit half-metallicity. The spin density in these half-metallic states is concentrated at the cluster edges, similar to the more typical expectations for h-BN/graphene intercalated nanoribbons. Based on the first principles findings of ref.45, the metallic heterostructures that

develop in BN-nanotubes during C-fullerene coalescence are a consequence of the electron transport channel provided by the core of corrugated C-nanotube.
The following brief summary should have given you enough information to draw some conclusions on the several suggested models of metallic conductivity in boron nitrides. These materials have very basic atomic structures and the chemical formula BN. Some of these models are associated with phase-inclusions, structural flaws, or impurities. On the other hand, the metallicity in boron-rich boron nitrides, which are generated at very high temperatures and have complicated clustered structures, cannot be explained by these theories.

Although all boron nitrides with the common stoichiometric composition BN are insulators, we have produced a conductive BNx with an excess of boron, where x << 1, in this study. A combination of various is used to mimic "metallic" boron nitride.

structural alterations to boron carbide and semiconducting boron, namely a structure made up of icosahedral and perhaps minor amounts of quasi-planar boron clusters, highly doped with nitrogen. The results of the quasi-classical approximation calculations show that nitrogen impurities in all-boron and boron-rich lattices produce electron donor states in the conduction band, which in turn cause local "metallization" of bonding.

Materials and Methods

The pyrolytic BN crucibles, which are filled with a powdered combination of boron and a metal oxide, are supported in our studies by high-purity pressed BN rods (Figure 1). Water vapour and ambient gas adsorptions were the only trace impurities in the 99.999 percent pure crystalline boron that was used. Throughout each synthesis cycle, the molten material was in constant touch with the crucible for many hours. The crucible remained excessively hot even one day after the power was turned off. Simply flipping the crucible would release the polycrystalline boride, whose mass was always far lower than the powder in the original room-temperature crucible.

Figure 1. Crucible and its support before the melting runs.

The deposits that accumulated during many melting sessions are shown in Figure 2. In one spot, we can make see the severely corroded rods that supported the crucible, which had much less damage. This must be because the BN materials used in rods and crucibles have varying degrees of structural defects; for example, graphite, which is readily reactive in high-purity pressed form, does not react in pyrolytic form; the material used in crucibles, with its tiling structure, provides almost little surface area for B to bind to.
The presence of B-vapor overflowing the pyrolytic BN crucible during the charge material's vacuum reduction at temperatures greater than 2050 °C clearly causes the highest-purity pressed BN rods, which are used to suspend the crucible in the ideal thermal position in the carbon vacuum furnace, to be aggressively attacked by residual B-vapor.

Figure 2. Deposits formed on rods and crucible during several melting runs.

Regarding the oxygen, it would have been pushed away by a turbo-molecular pump that was directly connected to the vacuum chamber. The pumping efficiency was optimised at about 10-6 Torr, and it would have partly sublimated from the metal oxide at much lower temperatures. The remaining oxygen, however, may either evaporate or form bonds with boron clusters; as a result, their deposit will likely include some oxygen as well. In an other instance, the molten boride attacked the crucible too aggressively when it was machined from the same high-purity pressed BN as the rods. Thermochemical assault was more successfully repelled by pyrolytic BN at these very high temperatures.

Figure 3 shows that a thin layer of silicon-colored material coated the rods and crucible after several successive melting sessions.

Figure 3. Rods and crucible entirely covered with silicon-colored deposit.

When the rods undergo severe erosion, they become unreliable and cannot hold the crucible any more; nonetheless, they may be used for melting runs until their diameter is too small (Figure 4).

Figure 4. When erosion of rods is very intensive, they are unable to support the crucible.

We believe that the BNx, x < 1 compound is what the irregular shells created around the rods are. This result is based on the fact that the shells' internal diameter remains constant with the pressed BN rods' initial diameter throughout the runs, whereas the rods' outer diameter decreases with each run, despite the fact that the shells progressively encase the rods. The seemingly thin BNx shells thickened in the interior dimension layer by layer, it seems. As the BNx shell collects the dissociated nitrogen, the structure is copied on the inner surface. This replication occurs after the BNx structure is created on the initial BN rod surface by reacting with excess B-vapor.

Extracted from the substance, the specimens had a glossy outside and a matte black inside. The reason for this might be because once the shell is shut, any gas inside the chamber cannot escape or be polluted.

In order to understand how the substance was formed, it is necessary to conduct thorough analyses of various experimental settings.

Phase transition temperatures are directly proportional to the fraction of boron atoms, therefore all metal atoms are strongly covalently bonded to some boron atoms at all times. Figure 5a displays the experimentally generated boride polycrystalline sample that was deemed to be the most ideal. However, in contrast to typical synthesis runs, when the boron atomic percentage hits the threshold range, the solid undergoes a drastic shrinkage and almost amorphous form, and the crucible contains very little material due to the extremely rapid rate of evaporation. It follows that boron, rather than metal, is donated to the vapour by boride inside the crucible. Additionally, there was no discernible metal peak or metal/boron peak in the ion spectra.

substances (for details on our previous mass spectrometry investigation of clusters generated by laser vaporisation of boride target rod, see this section).

(a)

(b)

Figure 5. Most perfect polycrystalline sample grown (a) after and (b) before being removed from the crucible.

The white line at the top edge of the crucible (Figure 5b) shows the completely unreacted, clean surface of the BN crucible, where the molten material remained constantly in touch throughout the phase shift. The layer of pure boron vapour above the crystal would have been a highly reflective, smooth band. The turbulence of the overflowing B-vapor-ambient-N interface zone is likely indicated by the irregular crystalline band at the top of the crucible, which is comparable to material developing on BN support rods and other exterior surfaces. Just like the samples that were examined, the "cap" disc that sits atop a rod is also identical.

To lessen the issue of carbon contamination, the pyrolytic BN crucible technique was developed as an alternative to graphite. If the crucible had included any carbon, it would have interacted with the minuscule amounts of oxygen and been expelled as a gaseous form as CO or CO2 under our harsh testing circumstances, which included temperatures above 2050 °C and pressures below 10-6 Torr. But it's reasonable to expect carbon in the final product because the vacuum furnace used ultra-purified graphite resistance-heating elements to heat the crucible to temperatures above 2000 °C. With a surface temperature closer to 3000 °C, the heating elements were undoubtedly white hot, meaning they sublimated carbon extensively. Furthermore, we had melted numerous times, which meant that the graphite

heating elements' surfaces had reacted with large amounts of the produced boron vapour. As a result, the inside surface was covered with small, hemispherical, glassy irregularities called "beads" that likely contained some

anything involving boron and carbon, or boron that is strongly doped with carbon. This source of carbon pollution should be diminished by such separation. However, inside the constraints of the furnace's insulating graphite fibre walls, there would be carbon in some form.
The surface's reflectance would reveal a polycrystalline morphology that is quite flat. Overflowing B-fluid from the crucible's top could only cause the silicon-colored shell's surface to continue accumulating boron. The outer surface is likely composed mostly of condensed boron clusters. The typical microstructure of these surfaces is shown in Figure 6.

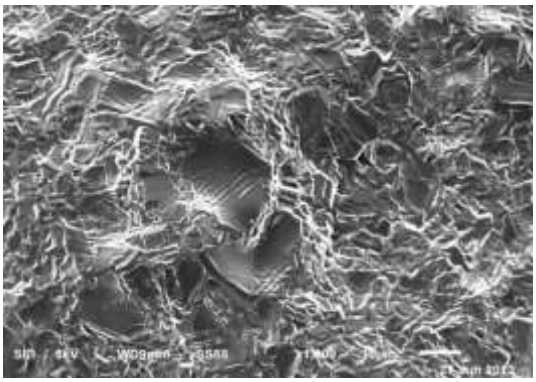

Figure 6. Outer surface microstructure of a shell.

The inner surface, on the other hand, would have expanded inwards, or towards the BN rod, which would be dissolving in almost gaseous convection-free nitrogen and boron vapour. The chemical makeup of the result would be more complicated than only BNx, however, due to the rods' contamination with carbon and maybe trace amounts of oxygen and other residual gases retained during pressing. The nitrogen most certainly comes from the pressed BN rods, not the pyrolytic BN crucible, since any outside supply of nitrogen at the chamber's base pressure of around 10-6 Torr would be in the parts per million range and therefore not a concern. Pictured in Figure 7 is the microscopic makeup of an interior surface. Droplets that have only partially fused together make up the bulk of the substance (Figure 8). However, flakes (Figure10) and threads (Figure 9) are also shown.

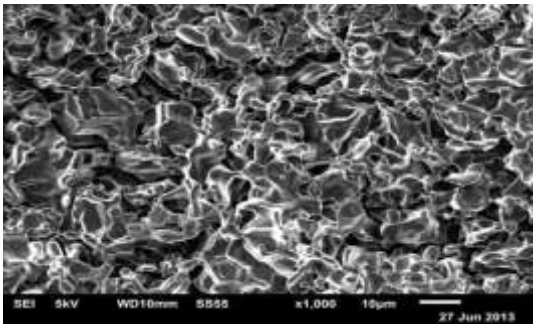

Figure 7. Inner surface microstructure of a shell.

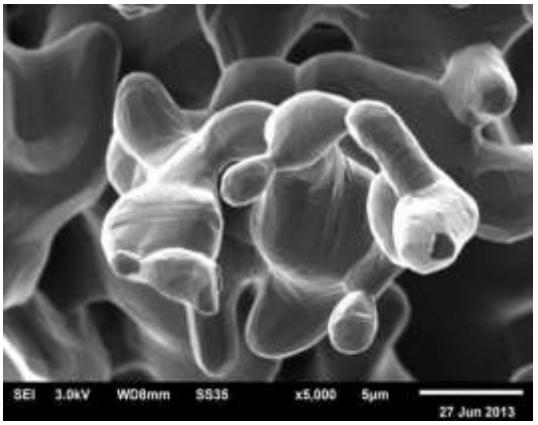

Figure 8. Microstructure built up from loosely fused droplets.

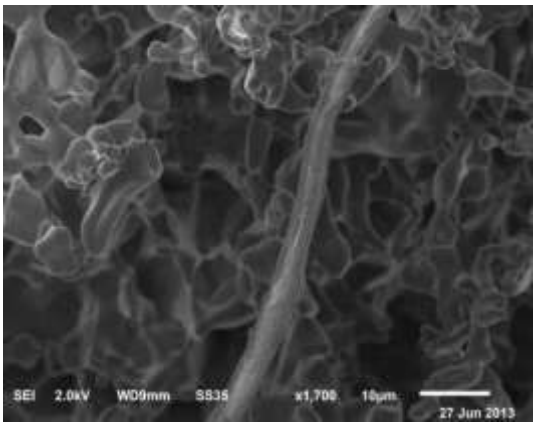

Figure 9. Thread presented in microstructure.

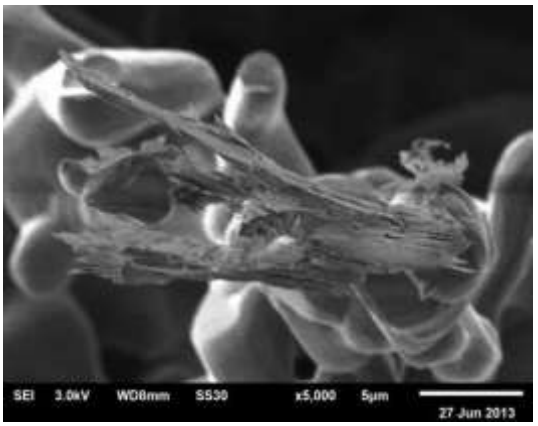

Figure 10. Flakes presented in microstructure.

When gaseous nitrogen is utilised instead of argon in other processes, for example during an implanter run, material with almost the same structure may be detected. The front surface of the ion source arc chamber, specifically with the boride target-crystal at the opposite end from the filament, was the intended location for this deposit. On the molybdenum sidewall, a thick and very hard black layer was created when nitrogen reactively spattered the crystal's surface. In most cases, a

combination of nano-allotropes was the end product. Another possible nitrogen source was associated with pressed BN dielectrics, which were substituted for the conventional corundum-made conical insulators used to support the boride target in the filament. Various sections of both glossy and dark surfaces had their chemical compositions examined. Figures 11 and 12 show examples of curves that are similar. Fragments having a flake-like form are the particular instance seen in Figure 13.

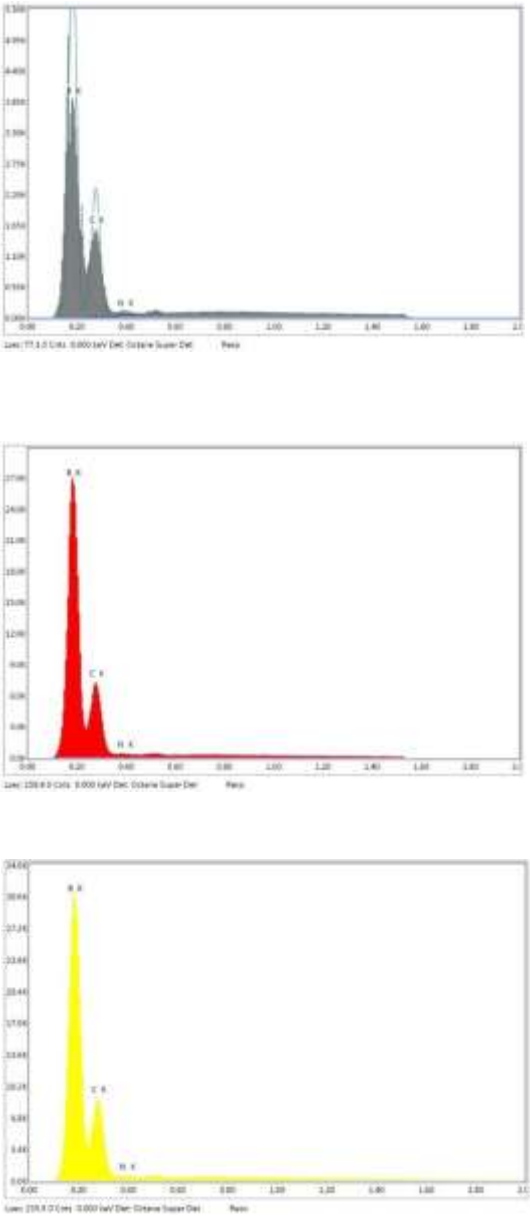

(a)

(b)

(c)

Figure 11. Chemical composition of a fragment of outer shell-surface: (a) unallocated, (b) B*K* / C*K* and (c) sum spectra.

Table 1 displays the numerical outcomes of this investigation. Evidence of almost uniform distribution of components on the surface is provided. B and C are the ones that are usually seen. The nitrogen concentration is low. We cannot discover O or any of the other trace elements. Regarding the inside, it shows that the chemical element distribution is rather uneven. While B and C concentrations stay high, N concentrations also reach a very high level.

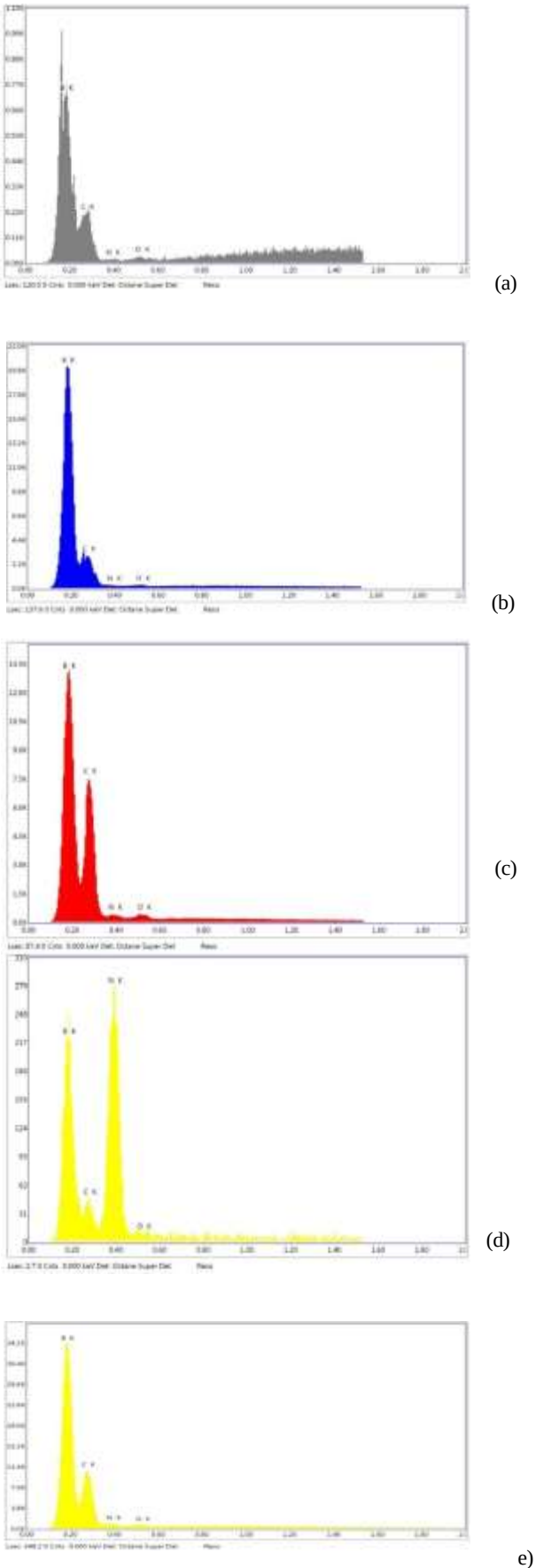

(a)

(b)

(c)

(d)

e)

Figure 12. Chemical composition of a fragment of inner shell-surface: (a) unallocated, (b, c) B*K* / C*K*, (d) N*K* /B*K* / C*K*, and (e) sum spectra.

Now O is a detectable element. It should be emphasized that highest concentration of N is characteristic for flake-like microstructures: B 55.31, N 40.21 and C 4.48 atom %, respectively.

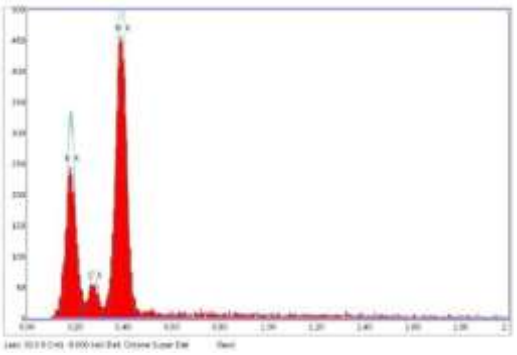

Figure 13. Chemical composition of flakes on inner shell-surface.

Tight electrical contact proved almost impossible to achieve without crushing the samples to dust as they are exceedingly delicate thin polycrystalline structures. The spring-loaded hook-clips made of brass served as the probes for the electrical measurements. Nevertheless, these samples were sometimes damaged even by the pressure they used, which was essential for getting a readout. This explains why our readings were so transient. Approximately 106 ohms is the range of the measured resistance R. We can recalculate the samples' resistivity using R ~ 106 Ω and rough estimations for the experiment's geometry, such as the distance between the probes l ~ 1 cm, their diameter d ~ 10^-1 cm, and the sample thickness w ~ 10^-2 cm.

$\rho = Rdw/l \sim 10^3$ Ω cm, which is significantly lower if compared with the room temperature intrinsic resistivity of insulating boron nitrides, e.g. h-BN: ~ 10^{13} Ω cm, or even semiconducting boron modifications, e.g. ground-state β-rhombohedral modification $B_{\sim 105}$ (β-B): ~ 10^7 Ω cm. Thus, obtained shells certainly are better conductive – "metallic" if compared with boron and boron nitride with chemical formula BN.

Table 1. Chemical composition of obtained shells in atom %.

Surface elements	Outer	Inner
B	85.66 – 88.57	55.31 – 91.00
N	00.34 – 00.67	00.01 – 40.21
C	11.09 – 13.57	04.48 – 18.15
O and other traces	00.00 – 00.00	00.00 – 00.77

The "metallicity" argument also includes the following: when placed on an insulating surface, shell fragments produce a circuit shortening effect; when a wall voltage is applied between two distant points on the surface of a shell fragment, the material is immediately vaporised with a blinding flash of light. Extensive testing was conducted on both surfaces and it was found that the shiny side made it more difficult to start an arc and produced weaker arcs than the black side, which was much more sensitive, vaporised more thoroughly, and produced brighter flashes. Thus, it is safe to state that the two surfaces vary significantly in electrical conductivity, with the

On the Positions of Nitrogen

The majority of the synthesised shells are boron, as may be stated.
Regarding the carbon content, it's above average but below the ~20% mark that is typical of boron carbides, which have the approximate chemical formula B4C. The unit cell of a boron carbide B12+xC3-x, where 0.1 < x < 1.7, is comparable to that of α-rhombohedral boron B12 (α-B), unless another elemental rhombohedron has extra C - B - C, C - B - B, or B - B- B atoms chains along its biggest diagonal. Thus, the substance must include α-B fine crystals and perhaps boron carbides with varying chemical make-ups (for information about the characteristics of crystalline boron and how they affect boron carbides, refer to reference 46).
In addition, it seems that the little β-B crystals are required. They may have trace amounts of carbon both dispersed in the lattice and separated at grain boundaries (up to a few atoms). Because carbon atoms easily replace boron atoms in too many regular sites, leading to the contraction of interatomic chemical bonds, it is practically impossible to accommodate carbon atoms inside the large crystallographic voids characteristic of the β-B lattice, thus we do not expect interstitial doping of β-B with C.

Lastly, the amorphous phase of boron (a-B) is eliminated throughout the synthesis process at very high temperatures. The only areas that may have a random structure in the material are tiny clusters of carbon-enriched boron that are either icosahedral or (quasi)planar.

black surface unquestionably being more conductive.

Thus, the synthesized shells can be imagined as a boron-based fine-structured multiphase system including α-B, β-B and traces of a-B doped with C, as well as boron carbides of different compositions. But, all these bulk phases are semiconducting. "Metallicity" of their mixture must be attributed to the presence of nitrogen with overly high concentrations. Consequently, we need to systemize here the data available on B/N systems for construction of the structural model describing position of N dopant atoms in the obtained material, which can be named as "boron-rich boron nitride."

B/N stoichiometries with B in excess

Solid structures, fullerenes, nanotubes, and boron nitride molecules and clusters all seem to choose stoichiometries high in boron.

Through the use of the Hartree-Fock (HF) approach, vibration spectra and optimal geometries for various B2N molecular states were derived.47 Statistical thermodynamic study reveals that B2N remains remarkably stable up to very high temperatures, in contrast to nitrogen-rich species BN2, which spontaneously dissociates to B + N2 regardless of

temperature. Solid BN and isolated noble gas matrices were vaporised by laser at helium temperatures to produce the BNB radical. Additionally, the theory's computation at the configuration-interaction (CI) level revealed this radical to be an exceptional stable linear species with the symmetric ground state. A number of B2N-related equilibrium states have

the Knudsen cell mass spectrometry that operates at high temperatures examined.49 The low-lying ionisation potentials and electron affinities of the strongly associated close- and open-shell molecules B2N and molecular ion B2N- were directly and accurately calculated using the Green's function-based method.
The finding of pure boron clusters Bn, where n ranges from 2 to 52, created by laser ablation of h-BN has been publicised.51 An empirical interatomic potential,52 parameterized by the LDA findings, may be used to describe the structures and energy of BnNm mixed clusters of B and N in a trustworthy way. The sputtering of BN with Cs or Rb indeed formed such clusters53. The mass distribution of the positive and negative products from the fragmentation of the anionic clusters in a gas target was used to determine the atom ordering in presumed linear species. It was shown that there are several anions with an excess of B, such as B2N, B3N, B4N, and B3N2. It is thought that these clusters are crucial building blocks for boron nitride thin films, nanoparticles, nanotubes, and nanomesh. In the visible spectral range, gas-phase electronic spectra of a few cyclic and linear BnNm radicals were recorded using a supersonic molecular beam.54 We theoretically derived a new set of graphite-like structures of BnNm clusters where n = m or n = m + 1 and where n + m ≤ 54.55

Boron nitride polyhedral compounds with face spirals may have their substitution isomers efficiently enumerated using a technique that was suggested 56. To count the related B24−mNm isomers with excess boron, i.e., m ≤ 12, it was applied to the fullerene-24 cage and the truncated octahedron. It is anticipated that species devoid of B-B or N-N bonds would exhibit stability comparable to carbon fullerenes. We investigated the structural properties and relative stability in B- and N-rich environments of various stoichiometric and non-stoichiometric boron nitride fullerenes with sizes varying from 28 to 128 atoms using first-principles calculations 57. The stoichiometric structures exhibit the highest degree of stability in B-rich environments for sizes greater than B16N16.

The arc discharge-synthesised boron nitride nanotube tips exhibited a "triangular flag" appearance. In addition to energetically favourable even-membered rings, this morphology also indicates the existence of odd-membered atomic rings. Rings with odd numbers form unlucky B-B or N-N bonds. Energy examination of distinct topologies of these boron nitride hetero-networks is necessary to differentiate between the two approaches of positioning the lines of unfavourable B-B or N-N bonds in this situation. A study was conducted on the adsorption of a single B-atom on the outside of zigzag BN nanotubes and hexagonal BN sheets using first-principles spin-polarized density-functional theory (DFT) calculations.
Some c-BN crystals exhibit a stoichiometric ratio B:N > 1, which is thought to be linked to the existence of free or bound B-impurities, such as B4C, B2O3, and BxO. This clarifies the reason for the unique growth conditions required for c-BN crystals with a reduced B-content.60

Varying levels of crystal structure perfection, clarity, and fineness of boron's behaviour during nitriding at

XRD (X-ray-diffraction), chemical analysis, and electron microscopy were used to study 61 materials subjected to extreme temperatures. An almost perfect yield of material with a BN-stoichiometric composition was not achievable following high-temperature nitriding.

We have studied the structural and phase changes of fine-grained h-BN powders that are heated in an optical furnace using a focused light beam of varying energy in a nitrogen flow.62 The surface observation of moulding powders revealed different structures of boron nitride as a consequence of the boiling process on the surface of an h-BN sample, which was caused by high-density radiation energy. A black porous melted drop containing amorphous phase of boron, h-BN, B2O3, and B2O is formed in the centre of the crater as a result of boiling and the thermolysis of h-BN with impurities of B2O3. It is expected that coarse whisker particles collected on a quartz substrate will form single-crystals of BN with an orthorhombic lattice. In subsequent steps, the BN nanostructures were created by subjecting fine-grained h-BN powders to light-induced heating in an optical furnace. This process included a stream of dried and purified nitrogen. Sublimated material may settle on a substrate as pure boron, amorphous BN, boron-rich tetragonal B51.2N, or B25N phases, according to studies of structure and phase composition. The use of pure boron powder as the initial material also results in the precipitation of amorphous structures, such as equiaxed nanoparticles and films with short needle-like nanostructures on the surface, according to studies of new BN nanomaterials obtained64 through concentrated light radiation heating in a high power optical furnace with a flow of commercially available nitrogen. Specifically, a process that occurs in a constant flow of nitrogen while the high power optical furnace is heated in its focus zone was studied.65 Whiskers (threads) around the crater and drips on the sample surface are initiated by the transition of BN nanotubes, as shown. There is a lot of B at the beginning of the whiskers and drops at the very beginning of their length. Extraction of the powder from the crater revealed that it contains amorphous boron nitride, equiaxed nanosized crystallites, thread-like structures (nanotubes and whiskers), h-BN crystals, and tetragonal phases B51N2 and B25N. The B-content is also elevated in this material. The material's band gaps were found to be 3.5, 3.8, and 4.8 eV, respectively, for the tetragonal B51N2 phase, the B25N phase, and the h-BN phase.

One way to make boron nitride is to use chemical vapour deposition (CVD) to deposit pure B onto carbon substrates, and then nitride those layers.66 Only in the presence of an

excess of N2 can the full conversion of B to BN be shown by thermodynamic analysis. How B and N respond in detail may be shown in the following ways: After attacking the B crystal, N atoms unite with B to create amorphous BN; at temperatures over 1200 °C, the BN undergoes a transformation into ordered ranged BN. An X-ray photoelectron spectroscopy (XPS)-based investigation into the impact of B-addition on the structure and mechanical properties of Al - Cr - N films grown by cathodic arc evaporation revealed the creation of a nanocomposite structure with a crystalline face-centered cubic Al - Cr - (B) - N solid solution and an

phase a-BNx, where x is less than 1.67, is amorphous. A BNx phase is probably forming, but the XRD pattern won't show it since it's usually amorphous. Spectra clearly show that when B content increases, the B - N peak becomes more intense and its percentage increases as well. An increasing proportion of the a-BNx phase with increasing B content may be used to interpret this.

Crystalline boron nitrides with B in excess

The B/N system, when heated to very high temperatures, produces a combination of phases containing an excess of boron and boron nitrides.

It was initially postulated in 1976,68 that this system may include boron subnitride B6N with an α-B-like structure by an analysis of the direct solid-diatomic gas interaction between boron and nitrogen in the high temperature region of 1480 to 1820 K. To produce BN from amorphous boron, which is likely to have an α-B-like structure, the reaction mechanism is probably topochemical, meaning that the rate is limited by the process happening at the interface between the two. In contrast, when β-B is the starting material, a two-step reaction series occurs, first with a homogenous reaction to form B6O, and then with a topochemical reaction to yield BN. Several boron subnitrides with various stoichiometries, such as B4N, were later identified; nonetheless, their structure and thermodynamic stability remained unknown.

The B13N2 rhombohedral boron subnitride was produced69 by cooling the B/BN melt to 5 GPa and then crystallising. This structure is an example of a kind that results from the interconnection of deformed B12 icosahedra via B-B bonds and N-B-N chains. The subnitride is a member of a class of boron-rich compounds having α-B-related structures, as shown by the Raman data. In comparison to BN phases of boron nitride, B13N2 is not as stable. In situ XRD using synchrotron radiation at high temperatures and pressures utilising a multi-anvil press was used to study the intricacies of chemical interaction and phase changes in the B/BN system. As the temperature rises over 2380 K, the β-B lines vanish because boron melts. A boron subnitride phase with a general stoichiometry of B12+xN2+y and a structure comparable to α-B is formed when samples with B6N and B5N compositions quenched from 2400 to 2600 K. The lines that correlate to a B6O-like lattice can be seen in the XRD patterns of the well-powdered quenched samples. An intermediate state between boron carbide B13C2 and boron suboxide B6O characterises the lattice characteristics of this boron nitride. In the B12+xN2+y phase, a three-dimensional structure is formed by twisted B12 icosahedra connected by N - B - N atomic chains. Having the same unit cell, space group, and atom sites as the subnitride, the most comparable compound is B4+zC1-z. The produced phase possesses the B13N2 stoichiometry because the atomic site occupancies are almost unitary across all crystallographic types. The as-synthesized B12+xN2+y subnitride's lattice parameter fluctuation was too minor in all studies to rule out the possibility that the ensuing phase B13N2 is a solid solution, unlike the boron carbide analogue. B13N2 crystallises in a mixture with β-B over the whole p - T -range that is being studied. This phase is comparable to the boron-rich tetragonal subnitride B50N2, which has a structure identical to the hypothesised first phase.

and h-BN, which are tetragonal boron ions. The proportion of B13N2 relative to the B50N2-like phase grows as the BN concentration in the initial mixture rises. Nevertheless, it seems that synthesising B13N2 in a single phase is not feasible, since its creation at around 5 GPa is governed by the liquid + h-BN ↔ B13N2 peritectic reaction. According to an in situ study71 that examined chemical interactions and phase relations in the B/BN system at pressures of approximately 5 GPa and temperatures up to 2800 K, a metastable liquid is formed in the system through contact interaction, as per the B + h-BN ↔ liquid eutectic reaction, with a temperature of 2120 K. After being heated to 2200 - 2250 K, the XRD patterns show the presence of B13N2 boron subnitride lines. It achieves eutectic equilibrium with B at 2300 K and 4% N, and it melts incongruently at 2600 K; no other boron subnitride is thermodynamically stable. A review compiled these findings on the high-pressure synthesis of new boron-rich solids, including boron-rich B/N phases.72 Using in situ experiments and thermodynamic simulations, researchers have studied the B/BN system's phase equilibria and found three distinct boron subnitrides. A report was made on the high pressure synthesis of the thermodynamically stable boron subnitride, which goes by the name B6N. But how it is structured remains a mystery. Based on the results of the simulations, it does not qualify as a member of the α-B12 family. Since it is only formed in the presence of BN, the second boron subnitride appears to be a B50N2−xBx solid solution, also known as an I-tetragonal boron, boron-rich quasi-periodic structure stabilised by nitrogen contamination. Its diffraction pattern is comparable to that of B50N2, and its lattice parameters match those predicted for B50N2. A powder XRD pattern similar to α-B12 was clearly seen when a third subnitride formed. The structure was solved and it is an example of a sort of structure that results from twisted B12 icosahedra connected by the N-B-N atomic chains. The phase has the stoichiometry B13N2. The only boron subnitride that was shown to be thermodynamically stable at around 5 GPa was rhombohedral B13N2. In accordance with the liquid + BN → B13N2 peritectic reaction, B13N2 melts at 2600 K in the phase diagram of the system that was created by adjusting the estimated equilibrium lines to the experimental data. At 2300 K, it forms a eutectic equilibrium with β-B~ 105. In a high-resolution transmission electron microscope

(HRTEM) with a scanning tunnelling microscope unit, the Joule-heating-induced failure of individual multi-walled BN nanotubes was studied. Upon further examination, it was determined that the failure mechanism included the internal thermal degradation of tubular layers, resulting in the formation of amorphous, ball-shaped nanoparticles composed of boron.

Local geometries in boron nitrides with B in excess

Given the foregoing, it is reasonable to assume that all boron nitride phases with an excess of B, including the one produced in this study, are really mixes of different boron modifications that are strongly doped with nitrogen. One possible local geometry for N atom environments in B/N systems rich in boron is the boron icosahedron B12, which is the primary structural motif of these crystals.

built using crystal structure information on B12-icosahedral networks studied, for instance, by Higashi and Ishii.74

Each corner of the rhombohedral unit cell in the α-B crystal is occupied by B12 icosahedra. Along the 5-fold axis, which runs parallel to the primary crystallographic axes, the icosahedra's linkages are impacted. The [111]-axis is characterised by translational periodicity in three icosahedral networks. From a crystallographic perspective, they are all identical, as they all lie parallel to the (111)-plane. Within each network, B12 icosahedra are connected by a bond with three centres. Conversely, 2-centered bonds along the 5-fold axes of icosahedra, perpendicular to the major crystallographic axes, connect icosahedral networks. Two nitrogen atoms are arranged on the [111]-axis in the α-B structure-type B12N2 (B6N) structure, with each atom serving as the centre of a triangle formed by three icosahedra B12 (see to Figures 14 and 15 for details). The addition of nitrogen atoms causes a little increase in the volume of the rhombohedral unit cell when the rhombohedral angle is varied. Albert and Hillebrecht gave the most up-to-date information on lattice parameters of a few structures linked to B6N.75

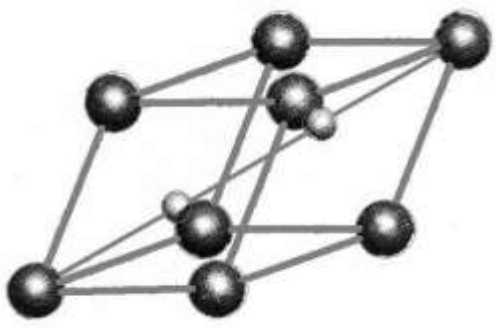

Figure 14. Structure of B_6N (α-B structure-type). Each circle at the lattice point stands for the B_{12} icosahedron and smaller ones on the [111]-axis are N atoms.

The α-tetragonal boron crystal structure is seen in Figure 16. Each unit cell contains four icosahedra of vitamin B12. They arrange themselves tetrahedrally around a single B atom in a perfect crystal form. Nevertheless, it has been suggested that the correct chemical make-up of this crystal phase might be B50N2, with N atoms substituting for the isolated B atoms in actual crystals. The icosahedral networks in α-tetragonal boron and B50N2 are identical, however.

Nitrogen in boron crystals

The investigations on γ-B doping, including N doping, have been summarised by us.76 What follows are the key findings. Nitrogen may be found in compounds with boron and can also fill up big spaces in the β-B lattice crystal structure. N is almost impossible to remove from β-B, much as other light elements.77 The distribution of nitrogen impurity atoms in β-B is not uniform, as shown by the microanalysis.

Figure 15. B_{12}-icosahedral network in the structure of B_6N as seen along the [111]-axis. The smaller circles stand for the N atoms.

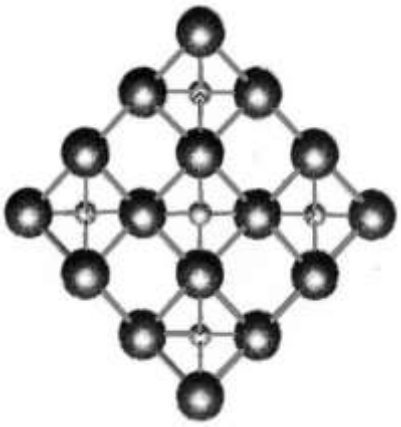

Figure 16. Structure of α-tetragonal boron as seen along the *c*-axis. The larger cycles stands for the B_{12} icosahedra and the smaller ones for the isolated N atoms. Each of the isolated N atoms is tetrahedrally coordinated with four icosahedra B_{12}.

A large number of crystallites and centres of crystallisation are formed when boron is melted in crucibles lined with boron nitride, contaminating the product with nitrogen.79 When β-B is melted in an environment that contains nitrogen, it forms very delicate samples. When these crystallites melt in BN crucibles, they encase a coarse-crystalline core and create a crust.80 Gaseous impurities such as H, N, and O were found in the β-B samples that were produced by zone-melting the compressed powders using H3BO3 as the binder material.81, 82 A fundamental tendency emerges from thermal-kinetic analysis: when the N concentration decreases, the O and H levels increase. In addition to increasing micro-strength and deformation energy, it reduces twinning. The concentration of unpaired spins increases in β-B crystals when nitrogen is diffused into the melt.It's 83,84 After undergoing high-temperature annealing, the corresponding electron-spin-resonance (ESR) line will vanish. The conductivity of β-B samples may be reduced by around by ~ 200 %.[85]

A low-energy-electron-diffraction (LEED) pattern, which is characteristic of the (111)-surface of β-B, was obtained[86] after heating at a temperature higher than 1400 °C. As indicated by Auger spectroscopy, this treatment is sufficient to eliminate O and C, the main impurities present on the initial surface. However, a certain amount of N remains on the surface. On heating up to 1200 °C, the LEED pattern showed a completely disordered surface structure. In order to obtain a clean surface, the material was subjected to heat treatment at > 1300 °C and the vacuum attained in the apparatus was better than ~ 10^{-9} Torr. These conditions are necessary for recrystallization (α ↔ β transition) of boron.

As shown by Auger spectrometry, O was below the sensitivity limits, but small amounts of C and N were presented. No peaks of other elements were found. The amount of C seems too low to affect the surface structure. As for the N, it can be removed only by ion bombardment with Ar ions, but N reappears after the high-temperature heating necessary in order to reobtain a regular surface structure. This indicated that N is segregated near the surface and it is not ruled out if N diffuses from the bulk. The minimum ratio between N and B Auger peaks was about 1 : 50. The surface covered by this contamination should be of the order of one-tenth of a monolayer what can affect the surface structure of the β-B.

In the work[87] curried out to study the interaction of fine grained boron powders with gaseous environment and develop a technique for removal of gases from powders, we determined the content of N_2 from the analysis by the reduction melting method. In powders with average particles sizes of 1.90, 0.46 and 0.25 μm, there were determined 0.9, 0.5 and 2.1 wt. % N_2, respectively.

Studying[88] the ion implantation in boron leads to the undisputable result that in the absence of a significant concentration (a few tenths atom %) of N no amorphization takes place in β-B implanted with N-ions. This result can be understood taking into account following two factors: (i) about ⅓ of the valence electrons in boron icosahedron are directed towards external bonds and their number and directions can be easily changed in order to adopt it to surroundings, giving rise only distortions from the regular configuration, and greater stability and versatility to the icosahedron; (ii) the β-B lattice affords eighteen vacant voids per hexagonal unit cell and can accommodate impurity concentrations of the stopping range of the order of $3 \cdot 10^{21}$ cm^{-3}. As for the boron nitrides of composition BN, whose structure is not built of icosahedra, they are known to be damaged very easily by irradiation even at very low doses.

Structural model of nitrogen-doped boron

Structural patterns of boron nitrides with excess of boron allow the constructing of the structural model for nitrogen impurity centers in boron matrix.

Previously, we reported[89] a mass spectrometric study of boron cluster anions B_n^-, $n \equiv 7 - 55$, containing multiple B_{12}-icosahedra, which were produced by laser vaporization both from pure boron (i.e. homogeneous) and boride (i.e. heterogeneous) target rods. While at lower masses these spectra were similar, at higher masses the boride spectrum exhibited a completely different pattern: in addition to the local maximum at B_{13}^-, characteristic of the pure boron spectrum as well, a repeating intensity pattern having local maxima at $(B_{13}^-)(B_{12})_2$ and $(B_{13}^-)(B_{12})_3$ as well as $(B_{13}^-)(B_{13})$ were observed. These observations can be attributed to the structural differences between the two target materials. The appearance of B_{12} units in the boride mass spectrum is presumably due to the ablation of relatively labile B_{12} cages from the structure. The fusion of two B_{12} units, followed by their asymmetric dissociation upon electron attachment into $B_{13}^- + B_{11}$ or $B_{11}^- + B_{13}$ explains why both clusters B_{13}^- and B_{11}^- display higher intensities than their immediate neighbors in both the pure boron and the boride mass spectra. As for the relative prominence of B_{13}^--based species over B_{11}^--based ones in the mass spectra, it may be due to B_{13} having a higher electron affinity than B_{11} and also stability of B_{13}^- with regard to electron loss. Further, we had demonstrated[90] that created boron clusters can be self-assembled into nanostructures.

Given the high carbon content, it is not completely out of the question that the synthesised material contains carbon-doped boron allotropes as well as boron carbide phases with crystalline lattices resembling α-B. These phases, like α-B, are semiconducting and contain all the other crystalline forms of boron. We can deduce the structure of potential atomic environments for N impurity atoms in synthesised material from these studies and the results given in the literature on B/N stoichiometries, crystalline boron nitrides, local geometries in boron nitrides with B excess, and nitrogen's behaviour in boron crystals.

Like the intralayer coordination in h-BN, the nitrogen atoms in B12N2 crystallites are encircled by three boron atoms that are symmetrically arranged in the same plane. Hence, we may use the length of the matching B-N chemical bonds, which is 1.45 Å, as an approximation. Although not exactly the same, crystallites of B12N2, α-B doped with N (i.e. with a maximum of one N atom per unit cell), and boron carbides doped with N (i.e. with a maximum of one or two B or C atoms per unit cell replaced with N atoms) would all exhibit comparable local environments.

B50N2 crystallites have four boron atoms around each nitrogen atom in a tetrahedral pattern, similar to the coordination in c-BN. This is why the length of the matching B-N bonds may be roughly estimated using the value of the c-BN bond, which is 1.57 Å.

Lastly, in β-B crystallites, nitrogen impurity atoms may be arranged in crystallographic voids of kinds A(1), A(2), A(3), D, and E. These types have 12, 12, 14, and 15 neighbouring boron atoms, and the average length of the B-N bonds is 2.17, 2.10, 2.15, 2.36, and 2.38 Å, respectively. Unless additional contaminants replace some of the N atoms and stabilise the structure, the situation must be quite similar in I-B crystallites.

As for the flakes found in our material, their layered structure and chemical composition with highest nitrogen and relatively low carbon contents and small excess of boron point to the local formations of h-BN doped with carbon (i.e. h-BNC) together with small amount of boron- rich phases doped with nitrogen.

Theorizing

Finding out the electron energy levels of dopant nitrogen accommodated in various boron-rich lattices requires development of a special model of impurity centers. The situation when the nitrogen atom is introduced among boron atoms, already tightly bonded together, essentially differs from that when a tightly bonded with neighbors constituent boron atom is substituted. Therefore, standard models for impurity centers cannot be used for our purposes. The appropriate model was proposed and successfully applied for β-B doped with metals by us earlier.[91] Taking into account that such an impurity atom only slightly affect the crystalline structure, within the first approximation the donor energy level of the impurity atom can be found from the outer valence shell ionization potential of the same chemical element in isolated state shifting the corresponding electron energy level in the internal crystalline field. This chemical shift can be found assuming that changes in the electric field within an impurity atom are determined mainly by the boron atoms directly surrounding it. Within the proposed model, the depth of the donor level E_D formed by the nitrogen impurity atom embedded in a certain boron-rich crystallite is determined from the relation

$$E_{\mathrm{D}} = (E_{\mathrm{IP}} + E'_{\mathrm{IP}}) - (E_{\mathrm{WF}} - E_{\mathrm{G}}) \qquad (1)$$

In this context, E'IP refers to the change in the crystallographic field of the N atom, EIP=14.53 eV, the electron work function (EWF) and the band gap (EG) of the semiconductor are also involved. With respect to ϰ-B, EWF= 6.13 eV and EG= 1.56 eV. Our evaluation of the available experimental data led us to this number for the work function. There is a lack of information on the job function of α-B and I-B. Assuming it is about the same for all crystalline variants of boron, we take the difference EWF - EG = 6.13 eV - 1.57 eV = 4.56 eV in all the instances following.

So, only one variable, E'IP, has to be calculated in order to locate the nitrogen donor levels on the energy axis. We may get an approximation for its value by using the quantum mechanical mean of the crystalline field's electron potential energy. The first quasi-classical approximation yields:

$$E'_{\mathrm{IP}} = -\frac{3NE_{\mathrm{IP}}}{4\pi(4n_{\mathrm{IP}}^2 - l_{\mathrm{IP}}(l_{\mathrm{IP}}+1))}\sqrt{\frac{2E_{\mathrm{IP}}}{n_{\mathrm{IP}}^2 - l_{\mathrm{IP}}(l_{\mathrm{IP}}+1)}}\sum_{i=1}^{i=q}\varphi_i V_i(r'_{\mathrm{IP}}, r''_{\mathrm{IP}}, d) \qquad (2)$$

Here N is the coordination number – number of boron atoms surrounding the impurity nitrogen atom, and d is the B – N bonds average length; function $V_i(r'_{\mathrm{IP}}, r''_{\mathrm{IP}}, d)$ denotes the volume of the intersection of i th layer of the boron atom with the layer of the nitrogen atom limited by the classical turning points radii r'_{IP} and r''_{IP} of the outer valence shell electron:

$$r'_{\mathrm{IP}} = \frac{n_{\mathrm{IP}} - \sqrt{n_{\mathrm{IP}}^2 - l_{\mathrm{IP}}(l_{\mathrm{IP}}+1)}}{\sqrt{2E_{\mathrm{IP}}}} \qquad (3)$$

$$r''_{\mathrm{IP}} = \frac{n_{\mathrm{IP}} + \sqrt{n_{\mathrm{IP}}^2 - l_{\mathrm{IP}}(l_{\mathrm{IP}}+1)}}{\sqrt{2E_{\mathrm{IP}}}} \qquad (4)$$

where n_{IP} and l_{IP} represent, respectively, the principal and orbital quantum numbers of the outer valence shell electron in the impurity atom. For nitrogen $n_{\mathrm{IP}} = 2$ and $l_{\mathrm{IP}} = 1$.

The function $V_i(r'_{\mathrm{IP}}, r''_{\mathrm{IP}}, d)$ is calculated as a linear combination of intersection volumes of 4 pairs of spheres:

$$V_i(r'_{\mathrm{IP}}, r''_{\mathrm{IP}}, d) = V(r_i, r''_{\mathrm{IP}}, d) + V(r_{i-1}, r'_{\mathrm{IP}}, d) - V(r_i, r'_{\mathrm{IP}}, d) - V(r_{i-1}, r''_{\mathrm{IP}}, d) \qquad (5)$$

Here the coefficient φ_i is the volume-average of the electric field potential in the i th radial layer of boron atom, q is the number of layers of the quasi-classical averaging. The parameters r_i and r_{i-1} are the external and internal radii of the i th layer of boron atom, respectively (assuming $r_0 \equiv 0$). For B atom the parameter $q = 5$. As for the r_i and φ_i, they are given in Table 2. Their numerical values have been calculated and tabulated in ref.[92] The function $V(r1, r2, d12)$ has a geometric meaning as the volume of an intersection of two spheres with radii r_1 and r_2 whose centers are at the distance d_{12} from each other. It is an algebraic piecewise continuous function. Explicit form of $V(r_1, r_2, d_{12})$ has been described.[93]

Table 2. Quasi-classical parameters of potential distribution in B atom.

i	r_i, a.u.	φ_i, a.u.
1	2.758476 E–2	+ 2.105468 E+2
2	5.098016 E–1	– 8.882329 E+0
3	7.441219 E–1	– 3.652920 E+0
4	4.021346 E+0	– 2.060720 E–1
5	4.337060 E+0	– 6.135348 E–4

Table 3. Parameters of N donor centers in boron crystals.

Structure	Site	*N*	*d*, Å	E_D, eV
α-B		3	1.45	– 5.2
	A(1)	12	2.17	–12.3
	A(2)	12	2.10	–14.0
β-B	A(3)	12	2.15	–12.8
	D	14	2.36	–11.1
	E	15	2.38	–12.1
I-B		4	1.57	– 8.7

As shown in Table 3, the computed electron energy levels and characteristics of the associated impurity centres are summarised. Consequently, all the donor levels connected to N, with an ED value less than 0, are located either within the conduction band or even higher than the vacuum level. With this background, it's important to remember that the negative energy levels of No one can ever be physically present in a virtual classroom. At sufficiently enough concentrations, these dopant atoms promote metallization of the material by supplying electrons to low-lying electron traps within the band gap and eventually to delocalized electron states at the bottom of the conduction band.
The current calculations mostly show that the N atoms in BNx donate electrons. From this qualitative standpoint, one may argue the same. Although it is less electronegative than nitrogen, boron is still among the most electronegative elements. This is why the electron density is moved from the boron atoms to the nitrogen atoms in typical boron nitrides (BN). In boron nitrides, the electronegativity of the boron component is greatly improved because the surplus boron atoms may form icosahedra and other multi-atomic clusters (BNx, x << 1). So, it is possible to move the electron density away from N-atom clusters and towards B-clusters.

We cannot rule out the possibility that some of the obtained material contains boron nanophases. As a general rule, metallic nanophases are anticipated.94 Supposedly, the so-called borophene, which is composed on planar hexagonal B36 clusters, must be entirely metallic, according to a recent proposal 95. But whether or not that quantity of nanoboron-component is sufficient to create a continuous conductive matrix is very questionable. Therefore, it seems that the metallization associated with nitrogen doping phases of semiconducting boron, and maybe boron carbide inclusions, is the most common.

Conclusion

To summarise, the "metallic" conductivity in boron nitride didped with metals is analogous to that in boron nitride with an excess of boron. This finding allows for the possibility of modelling the material in question as a mixture of boron phases highly doped with nitrogen impurity.

To that end, let's talk about superconductivity and metallic conductivity in boron crystals.
A long-standing question about the unexpected semiconductivity of β-B, which was predicted to be metallic based on band simulations, has now been resolved. This material contains an odd number of electrons in its regular unit cell.96 The issue pertained to

to the breaking of stoichiometry in this crystal: the presence of unfilled bands requires reconstruction of chemical bands.

The first principles calculations of the energy bands of B12 were conducted using an expansion of plane waves to determine that α-B must be a semiconductor, as indicated by a

high symmetry of the icosahedron. The metallic–covalent bonding conversion in boron can occur at sites other than the center of the icosahedron. In particular, when a vanadium V atom is doped in the certain-type crystallographic void of β-B, the bonding nature is converted from the covalent one to the more metallic one. A characteristic phenomenon in the V-doped β-B is the change of electrical conductivity from that of semiconducting hopping-type into metallic one by doping with only ~ 1 atom % V.[99] This unique conversion of electrical conductivity seems to be due to the local metallic–covalent bonding conversion. A high concentration of lithium Li (up to the composition $LiB_{5.8}$, i.e. 18 Li atoms per cell) was doped into β-B.[100] In Li- or Mg-doped β-B, electron doping was compensated by removing of interstitial B atoms and by generating of vacancies.

Theoretical exploration of a group of B_{12}-based materials, A_xB_{12}, with A = Li and Ca, and x = 1 – 4, was done[101] by performing LDA calculations of the electronic structure, including DOS, using the first principles pseudopotentials. Li-doped materials mostly demonstrate to be sufficiently stable, whereas it is shown that all calcium-doped materials are unstable, including Li_2CaB_{12}. These calculations showed essentially metallic behavior of stable and metastable Li_xB_{12}. Favorable superconducting properties were predicted for Li_3B_{12}, in the context of the sufficiently high DOS at the Fermi energy and obtained bulk modulus that is indicative of strong electron–phonon coupling.

An alternative route to achieve the superconducting state in boron-rich solids has been proposed, the hole-doping of B_{12} icosahedra.[102] For this purpose a prototype metallic phase of $B_{13}C_2$ was considered. It was shown that in this compound the boron icosahedral units are mainly responsible for large phonon frequencies and moderate electron–phonon coupling. It was suggested that relatively high critical temperature could be a general feature of hole-doped boron icosahedral solids.

Thus, boron, heavily doped with metal impurities, exhibits metallic conductivity and even superconductivity.

As for the boron “doped” with nitrogen, i.e., boron nitride with boron in excess, there is only single indirect experimental evidence of its “metallicity” mentioned above. It was predicted that superhard rhombohedral subnitride $B_{13}N_2$ might exhibit metallic conductivity. Unfortunately, the $B_{13}N_2$ crystallization by peritectic reaction in the studied

$p-T$ range did not allow the study of such properties. gap of width 1.427 eV.

The proposal is for a unified representation of B-based icosahedral cluster solids.98 As a result of the discrepancy between the icosahedral symmetry and the space periodicity,

these materials are likely to exhibit complex structures like giant unit cell crystals or quasi-crystals. They can also have metallic and covalent bonds, as B is at the boundary of these types of bonding in the Periodic Table. Lastly, their Fermi level can be in the deep pseudo-gap or at the high DOS position, depending on the nature of their atomic orbitals.

One might anticipate that these high-pressure phases can exhibit remarkable electronic and phonon transport properties, considering (i) the metallic behaviour and even superconductivity seen in boron-rich solids under high pressure and (ii) the outcomes of high-pressure synthesis of new boron-rich solids, such as boron-rich B/N phases, which were discussed earlier.
The current work's theoretical conclusions for N-doping boron quantitatively back up the previously proposed qualitative mechanism of electronic property alteration by doping. The inherent acceptor levels are first filled with electrons from donor impurities. The result is a rise in p-type hopping conductivity as the concentration of hole-hopping centres rises. After around half of these centres are full, however,

Both the hopping conductivity and the concentration of localised holes start to decline. The n-type conductivity begins to rise with larger dopant concentrations, when the electrons occupy all the acceptor centres of intrinsic origin. This inversion of conduction type occurs. Lastly, a semiconductor-to-semimetal transition, or metallization, may be achieved by doping boron with donor atoms at high enough concentrations.

References

[1]Chkhartishvili, L., Lezhava, D., Tsagareishvili, O., Gulua, D., *Proc. Police Acad. Georg.*, **1999**, *1*, 295-300.

[2]Chkhartishvili, L. S., *Phys. Solid State*, **2004**, *46*, 2126-2133.

[3]Chkhartishvili, L., Lezhava, D., Tsagareishvili, O., *J. Solid State Chem.*, **2000**, *154*, 148-152.

[4]Chkhartishvili, L., *J. Solid State Chem.*, **2004**, *177*, 395-399.

[5]Chkhartishvili, L., *Mater. Sci. Ind. J.*, **2006**, *2*, 18-23.

[6]Al'tshuler, A. M., Vekilov, Y. K., Umarov, G. R., *High Temp. High Press.*, **1976**, *8*, 635-662.

[7]Zhang, Zh., Guo, W., *Nano Lett.*, **2012**, *12*, 3650-3655.

[8]Zhang, Sh., Wang, Q., Kawazoe, Y., Jena, P., *J. Am. Chem. Soc.*, **2013**, *135*, 18216-18221.

[9]Hu, Sh., Zhao, J., Jin, Y., Yang, J., Petek, H., Hou, J. G., *Nano Lett.*, **2010**, *10*, 4830-4838.

[10]Srivastava, A., Sharma, M., Tyagi, N., Kothari, S. L., *J. Comput. Theo. Nanosci.*, **2012**, *9*, 1693-1699.

[11]Mousavi, H., J. Supercond. *Novel Magn.*, **2013**, *26*, 2905-2909.

[12]Owens, F. J., *Mol. Phys.*, **2011**, *109*, 1527-1531.

[13]Anota, E. Ch., Escobedo–Morales, A., Villanueva, M. S., Vázquez–Cuchillo, O., Rosas, E. R., *J. Mol. Modeling*, **2013**, *19*, 839-846.

[14]Du, A., Chen, Y., Zhu, Zh., Amal, R., Lu, G. Q. (M.), Smith, S. C., *J. Am. Chem. Soc.*, **2009**, *131*, 17354-17359.

[15]Terrones, M., Charlier, J.-C., Gloter, A., Cruz–Silva, E., Terrés, E., Li, Y. B., Vinu, A., Zanolli, Z., Dominguez, J. M., Terrones, H., Bando, Y., Golberg, D., *Nano Lett.*, **2008**, *8*, 1026-1032.

[16]Barone, V., Peralta, J. E., *Nano Lett.*, **2008**, *8*, 2210-2214.

[17]Lai, L., Lu, J., Wang, L., Luo, G., Zhou, J., Qin, R., Gao, Zh., Mei, W. N., *J. Phys. Chem. C*, **2009**, *113*, 2273-2276.

[18]Tang, P., Zou, X., Wang, S., Wu, J., Liu, H., Duan, W., *RSC Adv.*, **2012**, *2*, 6192-6199.

[19]Li, X., Wu, X., Zeng, X. Ch., Yang, J., *ACS Nano*, **2012**, *6*, 4104-4112.

[20]Wang, Y., Ding, Y., Ni, J., *J. Phys. Chem. C*, **2012**, *116*, 5995-6003.

[21]Alem, N., Ramasse, Q. M., Seabourne, C. R., Yazyev, O. V., Erickson, K., Sarahan, M. C., Kisielowski, C., Scott, A. J., Louie, S. G., Zettl, A., *Phys. Rev. Lett.*, **2012**, *109*, 126102 (1-5).

[22]Park, Ch.-H., Louie, S. G., *Nano Lett.*, **2008**, *8*, 2200-2203.

[23]Chen, W., Li, Y., Yu, G., Li, Ch.-Zh., Zhang, Sh. B., Zhou, Zh., Chen, Zh., *J. Am. Chem. Soc.*, **2010**, *132*, 1699-1705.

[24]Samarakoon, D. K., Wang, X.-Q., Appl. *Phys. Lett.*, **2012**, *100*, 103107 (1-4).

[25]Zhang, H. X., Feng, P. X., *ACS Appl. Mater. Interfaces*, **2012**, *4*, 30-33.

[26]Lopez–Bezanilla, A., Huang, J., Terrones, H., Sumpter, B. G., *J. Phys. Chem. C*, **2012**, *116*, 15675-15681.

[27]Lopez–Bezanilla, A., Huang, J., Terrones, H., Sumpter, B. G., *Nano Lett.*, **2011**, *11*, 3267-3273.

[28]Lopez–Bezanilla, A., Huang, J., Terrones, H., Sumpter, B. G., *Nano Lett.*, **2012**, *12*, 3879-3879.

[29]Guo, Y., Guo, W., *Nanoscale*, **2014**, *6*, 3731-3736.

[30]Anota, E. C., Gutiérrez, R. E. R., Morales, A. E., Cocoletzi, G. H., *J. Mol. Modeling*, **2012**, *18*, 2175-2184.

[31]Mousavi, H., Moradian, R., *Solid State Commun.*, **2013**, *153*, 17- 22.

[32]Berseneva, N., Gulans, A., Krasheninnikov, A. V., Nieminen, R. M., *Phys. Rev. B*, **2013**, *87*, 035404 (1-9).

[33]Zeng, J, Chen, K.-Q., Sun, C. Q., *Phys. Chem. Chem. Phys.*, **2012**, *14*, 8032-8037.

[34]Wang, Y., Ding, Y., *J. Phys. Chem. C*, **2013**, *117*, 3114-3121.

[35]Xue, Y., Liu, Q., He, G., Xu, K., Jiang, L., Hu, X., Hu, J., *Nanoscale Res. Lett.*, **2013**, *8*, 49-55.

[36]Yan, B., Park, Ch., Ihm, J., Zhou, G., Duan, W., Park, N., *J. Am. Chem. Soc.*, **2008**, *130*, 17012-17015.

[37]Batista, R. J. C., de Oliveira, A. B., Pereira, N. R., Paolini, R. S., Manhabosco, T. M., *J. Phys. Cond. Matter*, **2012**, *24*, 165501 (1-10).

[38]Nakamura, J., Nitta, T., Natori, A., *Phys. Rev. B*, **2005**, 72 205429 (1-5).

[39]Liu, Y., Wu, X., Zhao, Y., Zeng, X. Ch., Yang, J., *J. Phys. Chem. C*, **2011**, *115*, 9442-9450.

[40]Yu, Zh., Hu, M. L., Zhang, C. X., He, C. Y., Sun, L. Z., Zhong, J., *J. Phys. Chem. C*, **2011**, *115*, 10836-10841.

[41]Xiao, H. P., He, Ch., Zhang, Ch., Sun, L. Z., Peng, X., Zhang, K., Zhong, J., *Physica B*, **2012**, *407*, 4770-4472.

[42]Song, L., Balicas, L., Mowbray, D. J., Capaz, R. B., Storr, K., Ci, L., Jariwala, D., Kurth, S., Louie, S. G., Rubio, A., Ajayan, P. M., *Phys. Rev. B*, **2012**, *86*, 075429 (1-12).

[43]Zhou, Y., Wang, Zh., Yang, P., Gao, F., *J. Phys. Chem. C*, **2012**, *116*, 7581-7586.

[44]Menezes, M. G., Capaz, R. B., *Phys. Rev. B*, **2012**, *86*, 195413 (1-9).

[45]Li, X., Yang, W., Liu, B., *Nano Lett.*, **2007**, *7*, 3709-3715.

[46]Wang, L., Mo, Y., Rulis, P., Ching, W. Y., *RSC Adv.*, **2013**, *3*, 25374-25387.

[47]Martin, J. M. L., François, J. P., Gijbels, R., *Chem. Phys.*, **1989**, *90*, 6469-6485.

[48]Knight Jr., L. B., Hill, D. W., Kirk, T. J., Arrington, C. A., *J. Phys. Chem.*, **1992**, *96*, 555-561.

[49]Meloni, G., Baba, M. S., Gingerich, K. A., *J. Chem. Phys.*, **2000**, *113*, 8995-8999.

[50]Mahalakshmi, S., Yeager, D.L., *Mol. Phys.*, **2003**, *101*, 165-174.

[51]la Placa, S. J., Roland, P. A., Wynne, J. J., *Chem. Phys. Lett.*, **1992**, *190*, 163-168.

[52]Albe, K., Möller, W., Heinig, K.-H., *Radiat. Eff. Def. Solids*, **1997**, *141*, 85-97.

[53]Vandenbosch, R., *Phys. Rev. A*, **2003**, *67*, 52709 (1-5).

[54]Ding, H., Morse, M. D., Mailer, J. P., *Mol. Phys.*, **2007**, *105*, 1251-1261.

[55]Feng, Y., Fang, F., *Asian J. Chem.*, **2012**, *24*, 4012-414.

[56]Shao, Y., Jiang, Y., *J. Phys. Chem.*, **1996**, *100*, 1554-1558.

[57]Alexandre, S. S., Chacham, H., Nunes, R. W., *Phys. Rev. B*, **2001**, *63*, 045402 (1-5).

[58]Saito, Y., Maida, M., *J. Phys. Chem. A*, **1999**, *103*, 1291-1293.

[59]Li, L. L., Yang, S. Q., Yang, X. J., Xu, X. W., Tang, C. C., J. *Mol. Str.*, **2012**, *1020*, 183-187.

[60]Shulzhenko, A. A., Sokolov, A. N., *High Press. Res.*, **2000**, *18*, 345-351.

[61]Lyashenko, V. I., Ostrovskaya, N. F., Zelyavskii, V. B., Kurdyumov, A. V., Bartnitskaya, T. S., *Powd. Metall. Met. Ceram.*, **2003**, *42*, 189-194.

[62]Sartinska, L.L., Frolov, A. A., Koval', A. Yu., Danilenko, N. A., Timofeeva, I. I., Rud', B. M., *Mater. Chem. Phys.*, **2008**, *109*, 20-25.

[63]Sartinska, L.L., *Acta Mater.*, **2011**, *59*, 4395-4403.

[64]Sartinska, L. L., Voynich, E. V., Bloschanevich, O. M., Frolov, G. O., Koval', O. Yu., Danilenko, M. I., in *Proc. 7th Int. Conf. MEE*, IPMS, Kiev, **2012**, 129-129.

[65]Sartinska, L. L., Frolov, A. A., Andreeva, A. F., Voynich, Y. V., Kasumov, A. M., Frolov, G. A., Tinkov, V. A., Stonis, V. V., *Nano Studies*, **2012**, *5*, 89-102.

[66]Ye, F., Zhang, L., Liu, Y, Li, S., Su, M., Yin, X., Cheng, L., Prog. *Nat. Sci. Mater. Int.*, **2012**, *5*, 433-439.

[67]Tritremmel, C., Daniel, R., Lechthaler, M., Rudigier, H., Polcik, P., Mitterer, C., *Surf. Coat. Technol.*, **2012**, *213*, 1-7.

[68]Condon, J. B., Holcombe, C. E., Johnson, D. H., Steckel, L. M., *Inorg. Chem.*, **1976**, *15*, 2173-2179.

[69]Solozhenko, V. L., Kurakevych, O. O., *J. Phys. Conf. Ser.*, **2008**, *121*, 062001 (1-7).

[70]Solozhenko, V. L, Kurakevych, O. O., *J. Solid State Chem.*, **2009**, *182*, 1359-1364.

[71]Solozhenko, V. L., Kurakevych, O. O., Turkevich, V. Z., Turkevich, D. V., *J. Phys. Chem. B*, **2010**, *114*, 5819-5822.

[72]Kurakevych, O. O, Solozhenko, V. L., *High Press. Res.*, **2011**, *31*, 48-52.

[73]Xu, Zh., Golberg, D., Bando, Y., *Nano Lett.*, **2009**, *9*, 2251-2254.

[74]Higashi, I., Ishii, T., *Forma*, **2001**, *16*, 187-207.

[75]Albert, B., Hillebrecht, H., *Angew. Chem. Int. Ed.*, **2009**, *48*, 8640-8668.

[76]Gabunia, D. L., Tsagareishvili, O. A., Chkhartishvili, L. S., Tavadze, G. F., in *Proc. 8th Int. Cong. ETHTMA*, NSC KhPTI – PPC Contrast, Kharkiv, **2007**, 211-272.

[77]Tsagareishvili, G. V., *Jpn. J. Appl. Phys. Ser.*, **1994**, *10*, 21-24.

[78]Prudenziati, M., in *Boron and Refractory Borides*, Springer-Verlag, Berlin, **1977**, 241-261.

[79]Niemyski, T., Pracka, I., Szczerbiński, R., Frukacz, Z., in *Boron: Preparation, Properties, and Applications*, Plenum Press, New York, **1965**, 35-43.

[80]Starks, B. J., Medcalf, W. E., in *Boron: Synthesis, Structure, and Properties*, Plenum Press, New York, **1960**, 59-69.

[81]Tsagareishvili, G. V., Oganezov, K. A., Bairamashvili, I. A., Khvedelidze, A. G., Mazmishvili, G. A., Chepelev, V. V., Tabutsidze, M. L., *J. Less-Comm. Met.*, **1979**, *67*, 419-424.

[82]Tavadze, F. N., Lominadze, J. N., Khvedelidze, A. G., Tsagareishvili, G. V., Shorshorov, M. Kh., Bulichev, S. I., *J. Less-Comm. Met.*, **1981**, *82*, 95-99.

[83]Appenheimer, S., Niemyski, T., Jabłoński, R., *Electron Technol.*, **1970**, *3*, 29-33.

[84]Gaulé, G. K., Breslin, J. T., Pastore, J. R., Shutteleworth, R. A., in *Boron: Synthesis, Structure, and Properties*, Plenum Press, New York, **1960,** 159-174.

[85]Babaev, R.M., Iglitsyn, M. I., Kiskachi, Yu. A., Tilhonov, V. N., *Dev. Control Syst.*, **1969**, *8*, 49-49.

[86]Rovida, G., Maglietta, M., *J. Appl. Phys.*, **1973**, *44*, 3801-3082.

[87]Tsagareishvili, G. V., Bairamashvili, I. A., Oganezov, K. A., Tabutsadze, M. I., Tsagareishvili, O. A., J. *Less-Comm. Met.*, **1981**, *82*, 131-135.

[88]Schmirgeld, L., Zuppírolli, L., Brunel, M., Delafon, J., Templier, C., *AIP Conf. Proc.*, **1991**, *231*, 630-638.

[89]Xu, S.-J., Nilles, J. M., Radisic, D., Zheng, W.-J., Stokes, S., Bowen, K. H., Becker, R. C., Boustani, I., *Chem. Phys. Lett.*, **2003**, *379*, 282-286.

[90]Boustani, I, Becker, R., in *Proc. 9th Ann. Nanotechnol. Conf. & Trade Show*, NSTI, Boston, **2006**, MO 60.802.

[91]Chkhartishvili, L., Murusidze, I., Darchiashvili, M., Tsagareishvili, O., Gabunia, D., *Solid State Sci.*, **2012**, *14*, 1673-1682.

[92]Chkhartishvili, L., Berberashvili, T., *J. Electro Magn. Anal. Appl.*, **2010**, *2*, 205-243.

[93]Chkhartishvili, L. S., *Math. Notes*, **2001**, *69*, 421-428.

[94]Chkhartishvili, L., in *Boron: Compounds, Production and Application*, Nova Sci. Publ. Inc., New York, **2011**, 221-294.

[95]Piazza, Z. A., Hu, H.-Sh., Li, W.-L., Zhao, Y.-F., Li, J., Wang, L.-Sh., *Nat. Commun.*, **2014**, *5*, 3113 (1-15).

[96]Shirai, K., Uemura, N., *Solid State Sci.*, **2012**, *14*, 1609-1616.

[97]Lee, S., Bylander, D. M., Kleinman, L., *Phys. Rev. B*, **1990**, *42*, 1316-1320.

[98]Kimura, K., Hyodo, H., Takagiwa, Y., Kirihara, K., Soga, K., Kato, K., Takata, M., in *Abs. 17th Int. Symp. Boron, Borides & Rel. Mater.*, ITU, Istanbul, **2011**, 102-102.

[99]Soga, K., Hyodo, H., Iseki, H., Kimura, K., in *Abs. 17th Int. Symp. Boron, Borides & Rel. Mater.*, ITU, Istanbul, **2011**, 68-68.

[100]Hyodo, H., Nazu, A., Soga, K., Kimura, K., *Solid State Sci.*, **2012**, *14*, 1578-1583.

[101]Gunji, Sh., Kamimura, H., *Phys. Rev. B*, **1996**, *54*, 13665-13673.

[102]Calandra, M., Vast, N., Mauri, F., *Phys. Rev. B*, **2004**, *69*, 224505 (1-5).